CHEMISTRY
A EUROPEAN JOURNAL

DOI: 10.1002/chem.200601026

Inorganic–Organic Hybrid Structures: Open-Framework Iron Phosphite–Oxalates of Varying Dimensionality

Sukhendu Mandal and Srinivasan Natarajan*[a]

Abstract: Inorganic–organic hybrid structures belonging to the family of iron phosphite–oxalates have been prepared by employing hydrothermal methods. Their structures, determined by single-crystal X-ray diffraction, show a hierarchy within the family. While compounds **I** and **II** are low dimensional, **III**–**VI** have three-dimensional structures. Compound **I** has edge-shared ladders of iron phosphite with oxalate units hanging from the iron centers. Compound **II** has a layer structure with a honeycomb-like arrangement. The three-dimensional hybrid structures have the oxalate units connected in both in-plane and out-of-plane modes. A newly identified secondary building unit (SBU-7) and the oxalate units satisfying the valence and coordination requirements in the structure of **V** are novel and noteworthy structural features. Magnetic studies show that the dominant interactions between the iron centers are antiferromagnetic. Similar to other known hybrid structures, the phosphite–oxalate structures appear to show wide compositional and structural diversity.

Keywords: iron · magnetic properties · oxalates · phosphites · structure elucidation

Introduction

Compounds possessing open-framework structures have been extensively investigated for their many important applications in the areas of catalysis, sorption, and separation processes. Of the many families of compounds that have been prepared, the oxotetrahedral frameworks appear to be the dominant ones, as exemplified by the large number of aluminosilicate zeolite, aluminophosphate, and zincophosphate structures.[1] Recent research has shown that the phosphite group can be employed as a building unit in the formation of a new series of inorganic open-framework solids. Thus, phosphite networks of Zn,[2,3] Fe,[4,5] V,[6] and Cr,[7] have been prepared and their structures determined. The phosphite group, with three P–O bonds, can form unique networks that are not generally observed in the typical four-connected phosphate-based compounds. Multidentate organic ligands have also been incorporated in phosphate networks, thereby giving rise to a new family of inorganic–organic hybrid structures. In particular, the substitution of oxalates in metal phosphates has produced an interesting variety of structures. A large number of transition-metal phosphate–oxalates have been prepared and characterized during the last few years.[8–11] Although phosphate–oxalates have been prepared and characterized, research studies on phosphite–oxalates are few.[12] We have prepared six new phosphite–oxalate compounds of iron exhibiting a hierarchy of structures of varying dimensionality. The compounds, $[C_6N_2H_{14}]_2[Fe^{III}{}_2F_2(HPO_3)_2(C_2O_4)_2]\cdot 2H_2O$ (**I**), $[C_6N_4H_{21}]_2[Fe^{II}{}_4(HPO_3)_2(C_2O_4)_5]\cdot 5H_2O$ (**II**), $[Fe^{III}{}_2(OH)_2(HPO_3)_2(C_2O_4)]\cdot H_2O$ (**III**), $[C_2N_2H_{10}][Fe^{II}{}_2(OH)_2(HPO_3)_2(C_2O_4)]$ (**IV**), $[C_8N_4H_{26}][Fe^{III}{}_6(HPO_3)_8(C_2O_4)_3]\cdot 4H_2O$ (**V**), and $[C_5N_2H_{14}][Fe^{II}{}_4(HPO_3)_2(C_2O_4)_3]$ (**VI**), have been obtained by employing hydrothermal methods. The compounds possess one- (**I**), two- (**II**), and three-dimensionally (**III**–**VI**) extended structures. In this paper, we report the synthesis, structure, and characterization of the compounds.

[a] S. Mandal, Prof. Dr. S. Natarajan
Framework Solids Laboratory
Solid State and Structural Chemistry Unit
Indian Institute of Science
Bangalore-560012 (India)
Fax: (+91) 80-2360-1310
E-mail: snatarajan@sscu.iisc.ernet.in

Supporting information for this article is available on the WWW under http://www.chemeurj.org/ or from the author.

Results and Discussion

Structure of $[C_6N_2H_{14}]_2[Fe^{III}{}_2F_2(HPO_3)_2(C_2O_4)_2]\cdot 2H_2O$ (I): The asymmetric unit of **I** contains 42 non-hydrogen atoms, of which two Fe and two P atoms are crystallographically independent. The iron atoms are octahedrally coordinated

with five oxygen atoms and a fluorine atom. The average Fe–O/F bond length is 1.989 Å. Both Fe(1) and Fe(2) make three Fe–O–P bonds (average: 138.1°) and two Fe–O–C bonds (average: 115.3°) and possess one terminal Fe–F bond. Both of the P atoms make three P–O–Fe bonds. The P–O bond lengths have an average value of 1.519 Å. The C–O and C–C bond lengths and O–C–O bond angles are in the expected ranges. Selected bond lengths are given in Table 1.

The structure of **I** consists of a network of FeO_5F, HPO_3, and C_2O_4 units connected through the vertices to give rise to a one-dimensional structure. The FeO_5F and HPO_3 units, strictly alternating, are connected through oxygen atoms to form a simple four-unit-membered ring; these rings are connected edge-wise to form a one-dimensional ladderlike structure. The oxalate and fluoride ions are grafted onto this one-dimensional structure by bonding with the iron center. The doubly protonated amine molecule, 1,4-diazabicyclo-[2.2.2]octane (DABCO), occupies the interladder spaces and provides the charge balance (Figure 1). Both the terminal

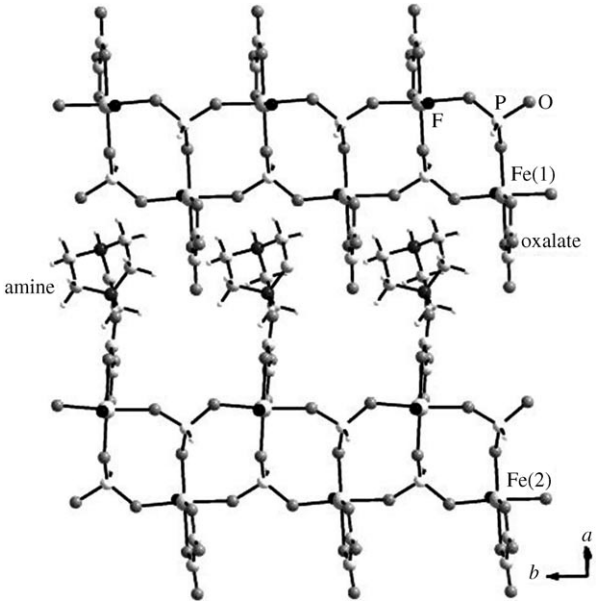

Figure 1. Structure of $[C_6N_2H_{14}]_2[Fe_2F_2(HPO_3)_2(C_2O_4)_2]\cdot 2H_2O$ (**I**) showing the one-dimensional ladder along with the DABCO molecules.

oxalate and fluoride ions participate in hydrogen bonding with the DABCO molecule. Thus, N–H···F, C–H···F, and C–H···O-type hydrogen bonds have been observed. The hydrogen-bond interactions between the iron phosphite–oxalates and the amine molecules give rise to a supramolecularly organized open structure, as shown in Figure 2. The important hydrogen-bond interactions are listed in Table 2.

Structure of $[C_6N_4H_{21}]_2[Fe^{II}_4(HPO_3)_2(C_2O_4)_5]\cdot 5H_2O$ (II): The asymmetric unit of **II** contains 34 non-hydrogen atoms, of which one P and two Fe atoms are crystallographically independent. The iron atoms are octahedrally coordinated

Table 1. Selected bond lengths in compounds **I–VI**.[a]

Bond	Length [Å]	Bond	Length [Å]
	I		
Fe(1)–F(2)	1.912(4)	Fe(2)–O(3)	2.005(5)
Fe(1)–O(7)	1.969(5)	Fe(2)–O(4)	2.027(6)
Fe(1)–O(6)	1.974(5)	Fe(2)–O(5)	2.042(5)
Fe(1)–O(8)	2.019(5)	P(1)–O(1)	1.509(6)
Fe(1)–O(9)	2.022(5)	P(1)–O(2) no. 1	1.510(5)
Fe(1)–O(10)	2.039(5)	P(1)–O(3) no. 2	1.527(5)
Fe(2)–F(1)	1.924(4)	P(2)–O (8) no. 3	1.521(5)
Fe(2)–O(1)	1.964(5)	P(2)–O(6) no. 4	1.522(5)
Fe(2)–O(2)	1.980(5)	P(2)–O(7)	1.525(5)
	II		
Fe(1)–O(1)	2.101(2)	Fe(2)–O(9)	2.138(2)
Fe(1)–O(2)	2.117(2)	Fe(2)–O(10)	2.185(2)
Fe(1)–O(3)	2.111(2)	Fe(2)–O(11)	2.211(2)
Fe(1)–O(4)	2.130(2)	Fe(2)–O(12)	2.209(2)
Fe(1)–O(5)	2.150(2)	P(1)–O(7) no. 1	1.515(2)
Fe(1)–O(6)	2.171(2)	P(1)–O(13)	1.509(2)
Fe(2)–O(7)	2.017(2)	P(1)–O(8)	1.534(2)
Fe(2)–O(8)	2.116(2)		
	III		
Fe(1)–O(1)	1.903(19)	Fe(1)–O(6)	2.106(19)
Fe(1)–O(2)	1.951(2)	P(1)–O(1) no. 1	1.511(2)
Fe(1)–O(3)	1.953(18)	P(1)–O(2)	1.517(2)
Fe(1)–O(4)	2.069(2)	P(1)–O(3) no. 2	1.534(19)
Fe(1)–O(5)	2.087(19)		
	IV		
Fe(1)–O(1)	2.061(2)	Fe(1)–O(6)	2.230(2)
Fe(1)–O(2) no. 1	2.063(2)	P(1)–O(2)	1.512(2)
Fe(1)–O(3) no. 2	2.118(2)	P(1)–O(3)	1.515(2)
Fe(1)–O(4)	2.171(2)	P(1)–O(1)	1.522(2)
Fe(1)–O(5)	2.206(2)		
	V		
Fe(1)–O(1)	1.931(3)	Fe(3)–O(16)	1.994(3)
Fe(1)–O(2)	1.959(2)	Fe(3)–O(17)	2.067(3)
Fe(1)–O(3)	1.944(2)	Fe(3)–O(18)	2.095(2)
Fe(1)–O(4)	1.993(2)	P(1)–O(2)	1.516(3)
Fe(1)–O(5)	2.095(2)	P(1)–O(8) no. 1	1.515(6)
Fe(1)–O(6)	2.133(2)	P(1)–O(14) no. 2	1.519(3)
Fe(2)–O(8)	1.949(2)	P(2)–O(16) no. 3	1.511(3)
Fe(2)–O(7)	1.940(2)	P(2)–O(1) no. 3	1.507(3)
Fe(2)–O(9)	1.962(2)	P(2)–O(7)	1.516(3)
Fe(2)–O(10)	1.973(2)	P(3)–O(3)	1.516(3)
Fe(2)–O(11)	2.122(2)	P(3)–O(10)	1.520(2)
Fe(2)–O(12)	2.135(2)	P(3)–O(13)	1.524(3)
Fe(3)–O(13)	1.950(2)	P(4)–O(9) no. 4	1.529(2)
Fe(3)–O(14)	1.962(3)	P(4)–O(15)	1.523(2)
Fe(3)–O(15)	1.977(2)	P(4)–O(4)	1.525(2)
	VI		
Fe(1)–O(1)	1.994(2)	Fe(2)–O(8) no. 2	2.100(2)
Fe(1)–O(2)	2.088(2)	Fe(2)–O(4)	2.105(2)
Fe(1)–O(3)	2.106(2)	Fe(2)–O(9) no. 2	2.153(2)
Fe(1)–O(4)	2.118(2)	Fe(2)–O(3)	2.239(2)
Fe(1)–O(5)	2.220(2)	P(1)–O(7)	1.508(2)
Fe(1)–O(6)	2.260(2)	P(1)–O(1)	1.521(2)
Fe(2)–O(7) no. 1	1.980(2)	P(1)–O(4) no. 3	1.531(2)

[a] Symmetry transformations used to generate equivalent atoms: For **I**: no. 1: $-x+{}^5/_2$, $y-{}^1/_2$, $-z+{}^1/_2$; no. 2: $-x+{}^5/_2$, $y+1/2$, $-z+{}^1/_2$; no. 3: $-x+1$, $-y$, $-z$; no. 4: $-x+1$, $-y+1$, $-z$. For **II**: no. 1: $-x$, $-y+2$, $-z+2$; no. 2: $-x+1$, $-y+1$, $-z+1$; no. 3: $-x$, $-y+2$, $-z+1$; no. 4: $-x+1$, $-y+1$, $-z+2$. For **III**: no. 1: x, $-y+{}^3/_2$, $z+{}^1/_2$; no. 2: $x-1$, y, z. For **IV**: no. 1: $-x+1$, $y+{}^1/_2$, $z+{}^1/_2$; no. 2: x, $-y+{}^1/_2$, $z-{}^1/_2$. For **V**: no. 1: $-x$, $-y+1$, $-z+2$; no. 2: $-x-{}^1/_2$, $y+{}^1/_2$, $-z+{}^3/_2$; no. 3: $x-{}^1/_2$, $-y+{}^1/_2$, $z+{}^1/_2$; no. 4: $x-{}^1/_2$, $-y+{}^1/_2$, $z-{}^1/_2$; no. 5: $x+{}^1/_2$, $-y+{}^1/_2$, $z-{}^1/_2$; no. 6: $-x+{}^1/_2$, $y+{}^1/_2$, $-z+{}^3/_2$; no. 7: $x+{}^1/_2$, $-y+{}^1/_2$, $z+{}^1/_2$; no. 8: $-x-{}^1/_2$, $y-{}^1/_2$, $-z+{}^3/_2$; no. 9: $-x+{}^1/_2$, $y-{}^1/_2$, $-z+{}^3/_2$; no. 10: $-x+1$, $-y+1$, $-z+2$. For **VI**: no. 1: x, $y-1$, z; no. 2: $x-1$, y, z; no. 3: $-x$, $y+{}^1/_2$, $-z+{}^1/_2$; no. 4: $-x$, $y-{}^1/_2$, $-z+{}^1/_2$; no. 5: $-x$, $-y+1$, $-z+1$; no. 6: x, $y+1$, z; no. 7: $x+1$, y, z; no. 8: $-x+1$, $-y+2$, $-z+1$.

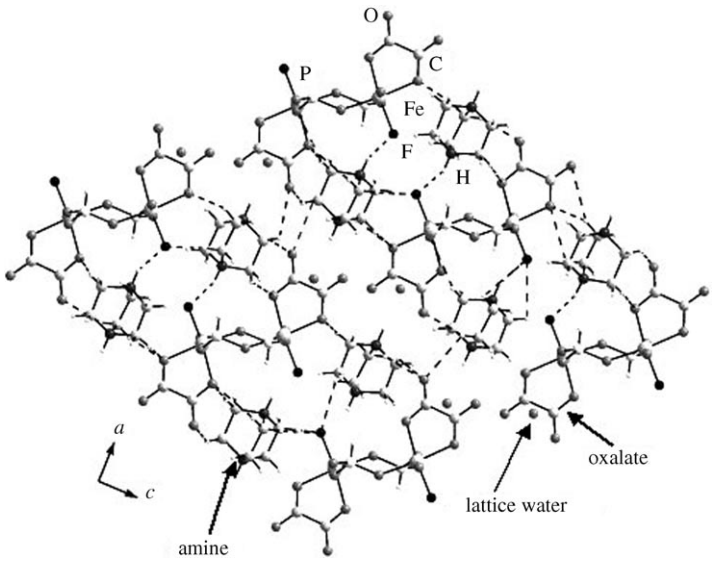

Figure 2. The three-dimensional hydrogen-bonded network formed between the ladders in **I**. Note that the amine molecules are situated within the channels. Dotted lines represent the possible hydrogen-bond interactions.

with six oxygen atoms (average: 2.138 Å). Of the two iron atoms, Fe(1) makes six Fe–O–C bonds (average: 113.9°) while Fe(2) makes two Fe–O–P bonds (average: 138.6°) and four Fe–O–C bonds (average: 114.5°). The P atom makes only two P–O–Fe bonds and possesses one terminal P=O. The P–O bond length has an average value of 1.519 Å. Selected bond lengths are given in Table 1.

The structure of **II** consists of a network of FeO_6, HPO_3, and C_2O_4 units. The structure can be considered to be essentially formed by the connectivity involving Fe and oxalate units in a layered honeycomb-like structure. The typical honeycomb structure, normally observed in transition-metal oxalates, is interrupted in **II** by the presence of the phosphite linkages.[13] In fact, two phosphite units connect two iron centers in exactly the same way as an oxalate unit would do (bidendate linkage). Thus, the bonding in **II** can be considered to be a distorted honeycomb-like structure (Figure 3). The organic cations and water molecules occupy the interlayer spaces and interact with the framework through N–H···O and C–H···O hydrogen-bond interactions (Table 2 and Figure 4).

Table 2. Important observed hydrogen-bond interactions in compounds **I**–**V**.

D–H···A	D–H [Å]	H···A [Å]	D···A [Å]	D–H···A [°]
		I		
N(1)–H(1)···F(1)	0.91	1.73	2.602(8)	160
N(4)–H(20)···F(2)	0.91	1.77	2.620(7)	154
C(1)–H(2)···O(4)	0.97	2.56	3.555(14)	152
C(2)–H(5)···O(14)	0.97	2.46	3.359(19)	155
C(5)–H(11)···F(2)	0.97	2.40	3.336(13)	161
C(6)–H(13)···O(9)	0.97	2.38	3.249(16)	148
C(9)–H(21)···O(10)	0.97	2.55	3.486(13)	163
C(11)–H(25)···O(5)	0.97	2.35	3.306(11)	167
C(11)–H(26)···O(12)	0.97	2.37	3.282(11)	156
		II		
N(2)–H(1)···O(9)	0.89	1.96	2.800(8)	156
N(2)–H(2)···O(8)	0.89	2.03	2.904(8)	166
N(2)–H(3)···O(13)	0.89	2.01	2.821(9)	151
N(1)–H(4)···O(13)	0.89	1.89	2.769(9)	169
N(1)–H(5)···O(8)	0.89	2.16	3.026(8)	164
N(3)–H(15)···O(6)	0.89	1.99	2.878(10)	173
N(3)–H(17)···O(13)	0.89	2.09	2.945(6)	161
C(2)–H(9)···O(1)	0.97	2.56	3.471(8)	156
		III		
O(4)–H(2)···O(6)	0.70	2.16	2.832	160
O(4)–H(3)···O(3)	0.78	2.03	2.802	174
		IV		
N(1)–H(1)···O(1)	0.89	2.05	2.926	168
N(1)–H(2)···O(2)	0.89	1.90	2.786	172
N(1)–H(2)···O(4)	0.89	2.20	3.057	162
C(1)–H(4)···O(5)	0.97	2.35	3.308	168
C(1)–H(5)···O(5)	0.97	2.42	3.371	167
		V		
N(1)–H(2)···O(2)	0.89	2.06	2.899(17)	157
C(1)–H(5)···O(6)	0.97	2.58	3.547(13)	179
C(2)–H(6)···O(7)	0.97	2.46	3.334(12)	150
C(4)–H(13)···O(5)	0.97	2.53	3.430(12)	154

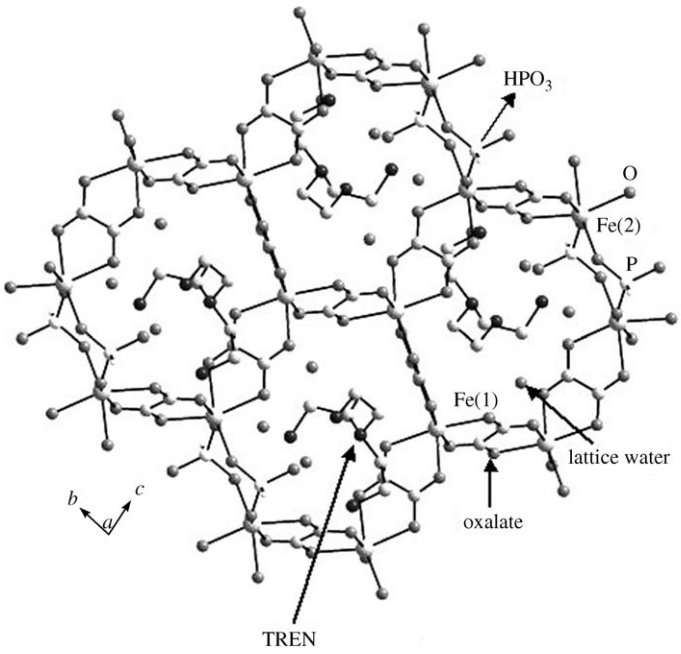

Figure 3. Structure of $[C_6N_4H_{21}]_2[Fe_4(HPO_3)_2(C_2O_4)_5]\cdot 5H_2O$ (**II**) in the *bc* plane showing the honeycomb-like structure. Note that two phosphite groups replace an oxalate unit. Hydrogen atoms on the amine molecules are not shown for clarity. TREN = tris(2-aminoethyl)amine.

Structure of $[Fe^{III}_2(OH_2)_2(HPO_3)_2(C_2O_4)]\cdot H_2O$ (III): The asymmetric unit of **III** contains 10 non-hydrogen atoms, in which one Fe and one P atom are crystallographically independent. The iron atom is octahedrally coordinated by six oxygen atoms with an average Fe–O bond length of 2.011 Å. The Fe(1) atom makes three Fe–O–P bonds (average: 149.1°), two Fe–O–C bonds (average: 114.1°), and one $Fe–O_{water}$ bond. The phosphorous atom is connected to two iron atoms through three P–O–Fe bonds. The P–O bond

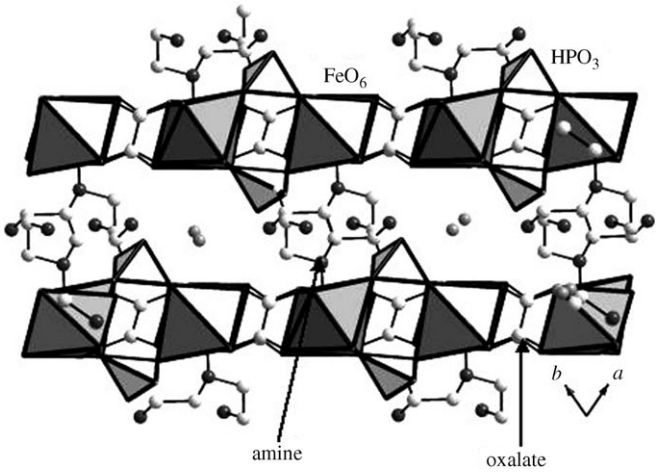

Figure 4. View of the layer arrangement in **II** in the *ab* plane. Note that the amine and the lattice water molecules occupy the interlamellar spaces. Hydrogen atoms on the amine molecules are not shown for clarity.

lengths have an average value of 1.520 Å. The observed bond lengths in **III** are listed in Table 1.

The structure of **III** is built from linkages involving the FeO_6, HPO_3, and oxalate units to give rise to a three-dimensional structure. The FeO_6 and HPO_3 units are connected in a layer with six-unit-membered apertures in the *ac* plane (Figure 5). The oxalate units act as pillars connecting the layers in an out-of-plane fashion to complete the three-dimensional structure (Figure 6). This connectivity gives rise to one-dimensional channels along the *a* axis wherein the bonded water and the extra-framework water molecules reside. The coordinated water molecules interact with the framework oxygen atoms through O–H···O hydrogen bonds (Table 2).

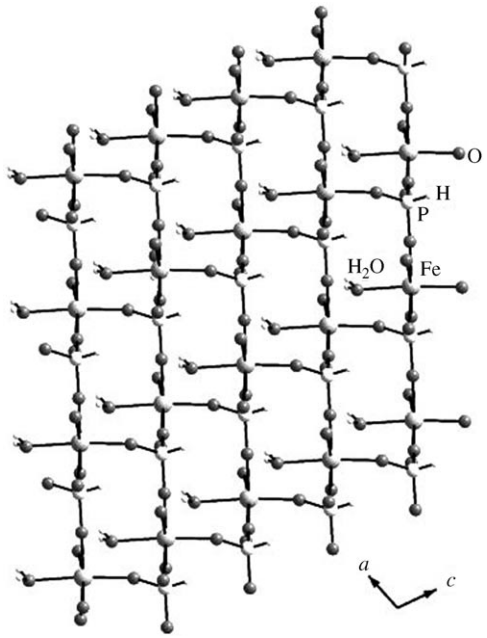

Figure 5. View of the inorganic layer in $[Fe^{III}_2(OH_2)_2(HPO_3)_2(C_2O_4)]\cdot H_2O$ (**III**). Note the formation of six-unit-membered apertures within the layers.

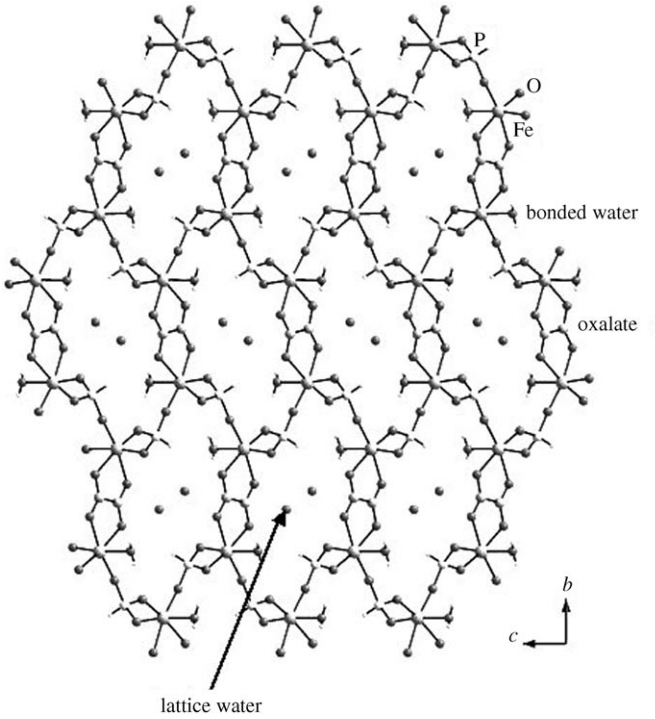

Figure 6. View of the structure of **III** showing the out-of-plane connectivity of the oxalate bridges. Note that the extra-framework water molecules occupy the channels.

Structure of $[C_2N_2H_{10}][Fe^{II}_2(OH_2)_2(HPO_3)_2(C_2O_4)]$ (IV): The asymmetric unit of **IV** contains 11 non-hydrogen atoms, in which one Fe and one P atom are crystallographically independent. The iron atom is octahedrally coordinated by six oxygen atoms with an average Fe–O bond length of 2.141 Å. The Fe(1) atom makes three Fe–O–P bonds (average: 133.6°), two Fe–O–C bonds (average: 113.7°), and one $Fe–O_{water}$ bond. The phosphorous atom is connected to three iron atoms through three Fe–O–P bonds. The P–O bond lengths have an average value of 1.516 Å. The observed bond lengths in **IV** are listed in Table 1.

The structure of **IV** consists of a network of FeO_6, HPO_3, and C_2O_4 units connected through their vertices to give rise to a three-dimensional structure. The strictly alternating FeO_6 and HPO_3 moieties are connected to form a two-dimensional layer with four-unit- and eight-unit-membered apertures in the *bc* plane (Figure 7). The water molecules bound to the iron center project into the eight-membered apertures. The oxalate units connect the layers in an out-of-plane fashion and complete the three-dimensional connectivity with eight-unit membered apertures along the *a* axis. The protonated ethylenediamine molecules occupy the one-dimensional channels and interact with the framework through N–H···O and C–H···O interactions (Table 2).

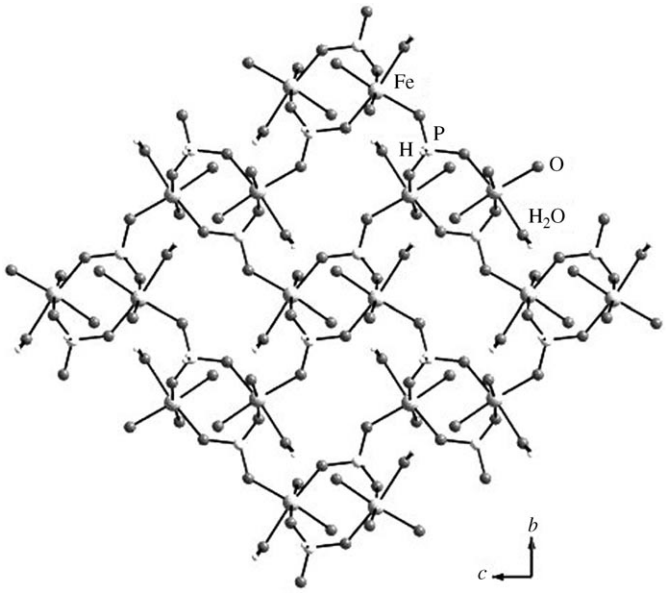

Figure 7. Structure of $[C_2N_2H_{10}][Fe^{II}_2(OH_2)_2(HPO_3)_2(C_2O_4)]$ (**IV**) in the *bc* plane showing the inorganic layers formed by four-unit- and eight-unit-membered apertures. (Contrast this arrangement with Figure 5 in which the layers are formed by six-unit-membered apertures only.)

Structure of $[C_8N_4H_{26}][Fe^{III}_6(HPO_3)_8(C_2O_4)_3]\cdot 4H_2O$ (V): The asymmetric unit of **V** contains 37 non-hydrogen atoms, of which three Fe and four P atoms are crystallographically independent. All the iron atoms are octahedrally coordinated with six oxygen-atom neighbors (average: 2.010 Å). The iron atoms make four Fe–O–P (average: 138.4°) and two Fe–O–C bonds (average: 113.7°). All of the P atoms make three P–O–Fe linkages. The P–O lengths have an average value of 1.519 Å. Selected bond lengths are given in Table 1.

The three-dimensional structure of **V** can be understood in terms of simpler secondary building units (SBU). Thus, the connectivity between the Fe(1), Fe(2), and Fe(3) octahedra and the P(1), P(2), and P(3) units results in the formation of edge-shared four-unit-membered dimers. The other phosphite group, P(4), caps one of the four-unit-membered rings of the dimer, thereby forming a new secondary building unit, SBU-7 (Figure 8a). The SBU-7 units are connected through terminal oxygen atoms to form a two-dimensional layer with alternating large and small apertures, as shown in Figure 8b. Within the small apertures, an oxalate unit connects two iron centers, mostly as a coordination requirement. The layers are further connected through oxygen atoms along the vertices, which gives rise to the three-dimensional structure. The oxalate units also link the layers by bonding with two iron centers of the adjacent layers (Figure 9). This is a truly remarkable structure, as the oxalate units appear to play an unusual dual role in contributing the necessary anionic charge for the valence considerations and satisfying the coordination requirements of the octahedral iron atom. The entire three-dimensional structure of **V** can be evolved through a simple Fe and P connectivity through bridging oxygen atoms, similar to many iron phosphate structures. The connectivity gives rise to one-dimensional channels with a size of 12.3×5.8 Å (longest atom–atom contact distances not including the van der Waals radii), in which the protonated amine molecules and the extra-framework water molecules are located. Hydrogen-bond interactions between the framework and the organic molecules have been observed (Table 2).

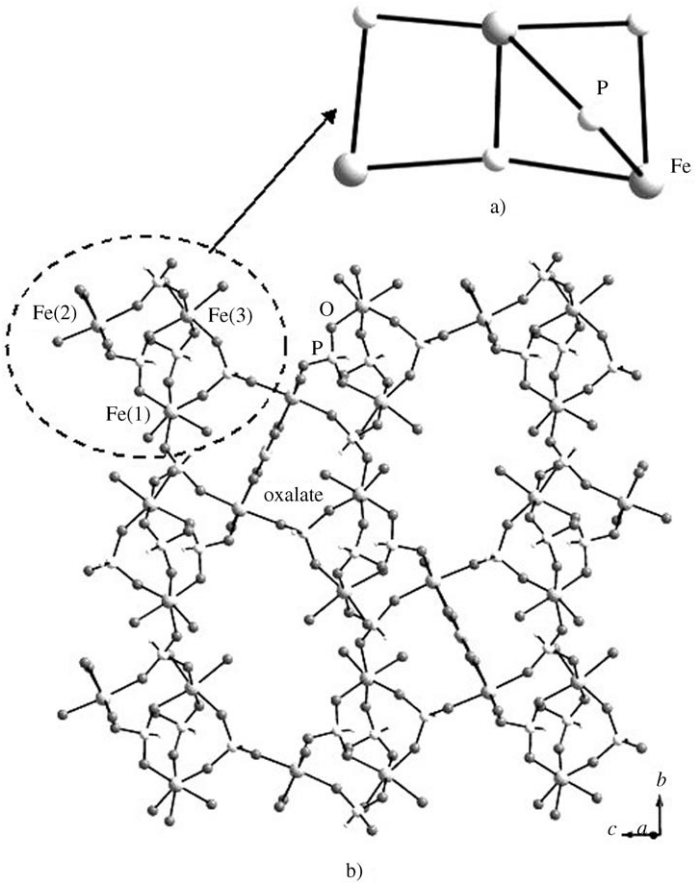

Figure 8. a) The SBU-7 unit observed in **V**. For the sake of clarity, the oxygen atoms are not shown and the Fe and P atoms are bonded directly. b) View of the two-dimensional structure in **V** in the *bc* plane.

Structure of $[C_5N_2H_{14}][Fe^{II}_4(HPO_3)_2(C_2O_4)_3]$ (VI): The asymmetric unit of **VI** contains 19 non-hydrogen atoms, of which one P and two Fe atoms are crystallographically independent. The Fe(1) atom is coordinated with six oxygen atoms (average: 2.131 Å) and the Fe(2) atom is coordinated with five oxygen atoms (average: 2.115 Å). The Fe(1) atom makes two Fe–O–P (average: 127.8°) bonds and four Fe–O–C bonds (average: 114.4°), while the Fe(2) atom makes two Fe–O–P bonds (average: 132.9°) and three Fe–O–C bonds (average: 123.1°). The two iron atoms are also connected to each other through three-coordinated oxygen atoms (O(3) and O(4)) with an average Fe–O–Fe bond angle of 101.07°. The P(1) atom makes three P–O–Fe linkages. The P–O lengths have an average value of 1.520 Å. Selected bond lengths are given in Table 1.

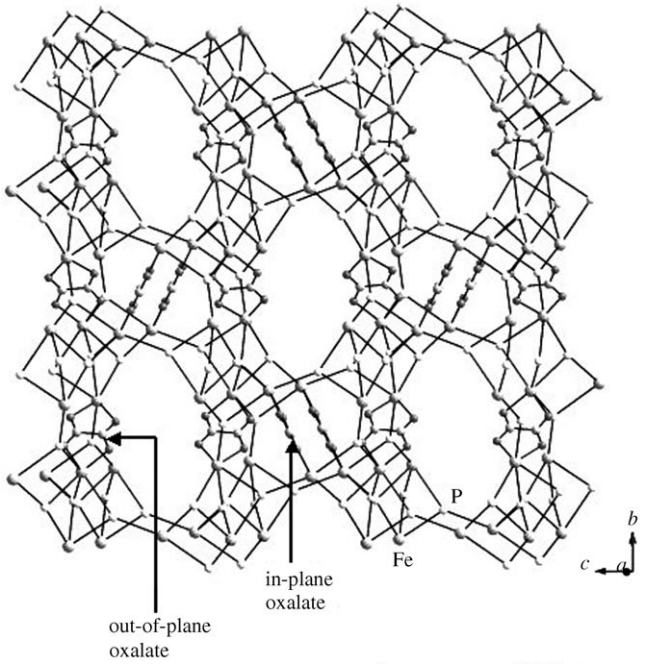

Figure 9. The T-atom connectivity (T = Fe or P) along with the oxalate units in the *bc* plane forming the three-dimensional structure in **V** (the oxygen atoms are not shown for clarity). Note that the oxalates units have both in-plane and out-of-plane linkages (see the text for further details).

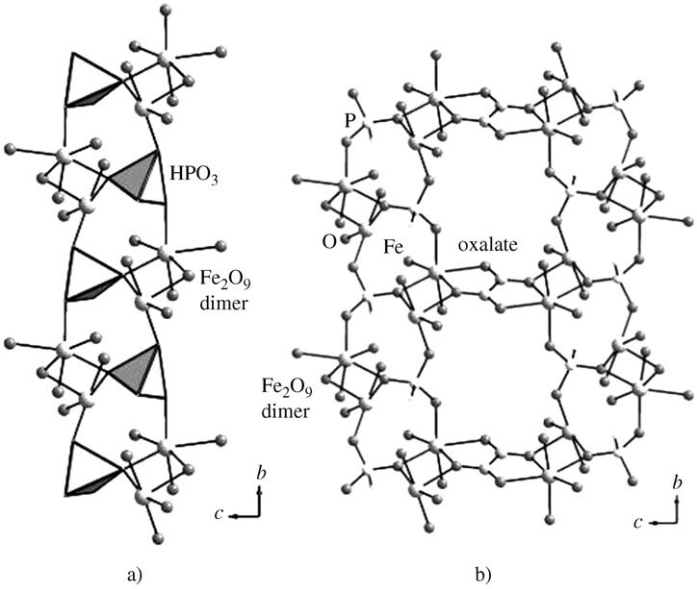

Figure 10. a) The one-dimensional structure formed by the linkage between Fe_2O_9 dimers and phosphite units. b) View of the hybrid layer structure in **VI** formed by the connectivity between the one-dimensional chains and the oxalate units (in-plane connectivity).

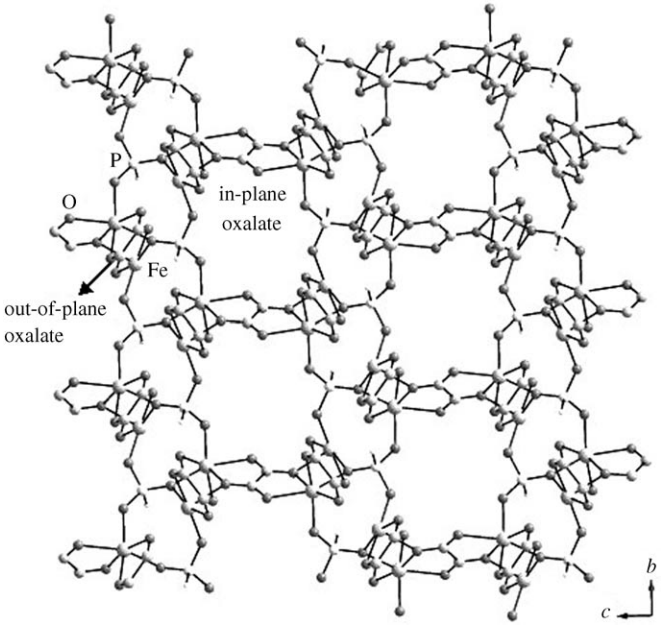

Figure 11. The three-dimensional structure of **VI** showing both the in-plane and out-of-plane oxalate linkages in the *bc* plane.

The framework structure of $[C_5N_2H_{14}][Fe^{II}_4(HPO_3)_2(C_2O_4)_3]$ (**VI**) comprises a network of FeO_6 octahedral, FeO_5 square pyramidal, HPO_3 pseudotetrahedral, and C_2O_4 units connected through their vertices to form the three-dimensional structure. The $Fe(1)O_6$ and $Fe(2)O_5$ polyhedral units are connected by two three-coordinated oxygen atoms, O(3) and O(4), forming an edge-shared dimer of the formula Fe_2O_9. The dimers are linked with the HPO_3 units to form one-dimensional structures (Figure 10a), which are connected by oxalate bridges, thereby giving rise to the two-dimensional structure (Figure 10b). The two-dimensional layers are further linked by oxalate units in a direction perpendicular to the plane of the layer to complete the three-dimensional connectivity. Thus, there are two types of oxalate units in **VI**, one connecting within the plane (in-plane) and forming the hybrid layers and the other connecting the hybrid layers (out-of-plane; Figure 11). This type of connectivity gives rise to one-dimensional channels with a size of 6.5×5.3 Å (longest atom–atom contact distances not including the van der Waals radii). The disordered homopiparazine molecule occupies the middle of the channel.

The iron phosphite–oxalates **I**–**VI** are members of a family of inorganic–organic hybrid framework structures. They have been obtained as good-quality single crystals by employing hydrothermal methods. Although all of the materials involve bonding between the iron centers, the phosphite groups, and the oxalate units, they exhibit distinct differences. While **I** is one-dimensional, **II** is two-dimensional and **III**–**VI** are three-dimensional in nature. In the case of **III**, although the synthesis was carried out in the presence of organic amines, the structure of **III** is formed without the amine molecules. Similar behavior has been observed before.[14,15] The unpredictable nature of the kinetically controlled solvent-mediated hydrothermal reactions is well illustrated by the formation of different phases of varying dimensionality along with the changes in the oxidation state of the iron.

It is pertinent to note that low-dimensional hybrid structures are rare in the literature.[16,17] Compound **I**, to the best our knowledge, is the first one-dimensional iron phosphite–oxalate structure. The present compound appears to be related to the iron arsenate–oxalate structure, $[C_4N_2H_{12}][Fe(OH)(HAsO_4)(C_2O_4)]\cdot H_2O$.[16] The basic one-dimensional structures in both the cases are similar. In the iron arsenate–oxalate, the OH and oxalate groups hang as pendants from the iron center, whereas in **I** we have the F^- ion replacing the OH group. The structure of **I** also has close similarities with the structure of the vanadyl phosphate–oxalate $[C_4N_2H_{12}][VO(HPO_4)(C_2O_4)]$[17] and with the structure of the iron phosphate-phosphite $[Fe^{III}(2,2'\text{-bipyridine})(HPO_3)(H_2PO_4)]$.[18]

The structure of **II** is unique and no known examples of such structural types exist in the literature. The formation of honeycomb oxalate networks templated by organic amines, based purely on bivalent transition metals, is very rare.[13] Usually, trivalent transition-metal oxalates form with the honeycomb structure.[13] The formation of honeycomb layers in amine-templated Zn^{II} oxalates has been known.[19] Presently, in **II** we have stabilized a honeycomb-like structure with bivalent iron. In **II**, in order to stabilize the honeycomb structure, two phosphite groups link with the iron centers, thereby completing the two-dimensional network. It is likely that the presence of the phosphite groups may be responsible for the observed unusual structural feature in **II**. Typically of honeycomb-layered structures, the layers in **II** are arranged in an AAAA··· fashion. The stacking of the layers gives rise to a one-dimensional channel system with the channels penetrating the structure in a direction perpendicular to the sheets. The interlayer separation is $\approx$6.3 Å. Similar interlayer separations have also been observed in layered iron and manganese phosphate–oxalates.[20]

The structure of **III** is similar to the iron phosphate–oxalate $[Fe_2(H_2O)_2(HPO_4)_2(C_2O_4)]\cdot H_2O$, previously reported in the literature.[8] The phosphite group in **III** replaces the phosphate group in $[Fe_2(H_2O)_2(HPO_4)_2(C_2O_4)]\cdot H_2O$. The formation of six-unit-membered apertures within the inorganic layers pillared by the oxalate units in an out-of-plane fashion appears to be common to both structures. The formation of six-unit-membered apertures within layers is considerably rarer, having been observed in only a very few systems.[8,14,21] The structure of **IV** also possesses inorganic layers connected by out-of-plane oxalate units. The layers in **IV** are formed by four-unit- and eight-unit-membered apertures. Four-unit- and eight-unit-membered apertures are commonly observed in many phosphate and phosphite networks.[22,23]

The hybrid structure of **V** has a unique connectivity. In **II**, we have a situation in which the structure was formed predominantly by oxalate units linking the iron centers and in **V** we have the entire network structure based upon the connectivity between Fe and P atoms through oxygen-atom linkages. The oxalate unit appears to perform the job of completing the coordination requirements of the octahedral iron atom, in addition to providing the necessary charge-balancing requirements for **V**. This dual role of the oxalate unit has never been observed in any of the hybrid structures reported in the literature. Additionally, the observation of a new secondary building unit, SBU-7, is also noteworthy. Ferey has proposed a set of secondary building units to explain and understand the complex three-dimensional structures based on octahedral–tetrahedral primary building units.[24] The present building unit, SBU-7, to our knowledge, is unique and no known examples exist in the literature. We have recently observed another type of SBU-7 in a zinc phosphite, $[(C_4N_2H_{12})(C_5NH_4)]_4[Zn_6(HPO_3)_8]$,[23] in which a six-unit-membered ring is capped by a phosphite group.

In the structure of **VI**, the single iron site is replaced by Fe_2O_9 dimers. The formation of Fe_2O_9 dimers in hybrid compounds is not uncommon, having been observed in $[C_4N_2H_{12}][Fe^{II}{}_4(HPO_4)_2(C_2O_4)_3]$[25] and $[C_4N_2H_{12}][Co^{II}{}_4(HPO_4)_2(C_2O_4)_3]$.[26] Thus, **VI** closely resembles both of these structures. The structure of **VI** is also closely related to the iron phosphite–oxalate $[C_4N_2H_{12}][Fe^{II}{}_4(HPO_3)_2(C_2O_4)_3]$, which was reported recently.[12] In the structure of $[C_4N_2H_{12}][Fe^{II}{}_4(HPO_3)_2(C_2O_4)_3]$, two octahedral Fe centers are connected through their edges to form Fe_2O_{10} dimers, which are again connected through their corners, thereby forming Fe–O–Fe one-dimensional chains. In **VI**, we have FeO_6 and FeO_5 units forming the Fe_2O_9 dimers, which are isolated.

The temperature variations of the magnetic-susceptibility studies indicate strong antiferromagnetic interactions in all of the pure phases, with the Neel temperatures in the range of 20–50 K (Figure 12 and Table 3). In all cases, the high-temperature magnetic behavior obeys the Curie–Weiss law. The calculated effective magnetic moment (μ_{eff}) at room temperature indicates that the iron is present in the high-spin state in all of the compounds and corresponds to the calculated moment based on the respective oxidation states (Fe^{2+} in **II** and Fe^{3+} in **I**, **III**, and **V**). In all of the compounds, the magnetic susceptibility (χ_m) increases with temperature, reaches a maximum, and then decreases. The temperature at which the maximum χ_m value occurs is that at which the antiferromagnetic ordering has set in for the compound. At high temperatures, the susceptibility value saturates to the paramagnetic-spin-only value of a Fe^{2+}/Fe^{3+} spin. A Curie–Weiss fit of the high-temperature data (T= 100–300 K) to the form $\chi=(C/T-\theta)$ gives values of C and θ for all of the compounds. The various observed and fitted magnetic parameters are given in Table 3.

Conclusion

Six new iron phosphite–oxalates belonging to the hybrid inorganic–organic family of open-framework structures have been synthesized hydrothermally in the presence of structure-directing organic amines. The oxalate unit in these compounds performs many roles. In **I**, it is just a terminal moiety, while in **II**, the oxalate units connect the Fe centers to form a honeycomb-like layered structure. In **III** and **IV**,

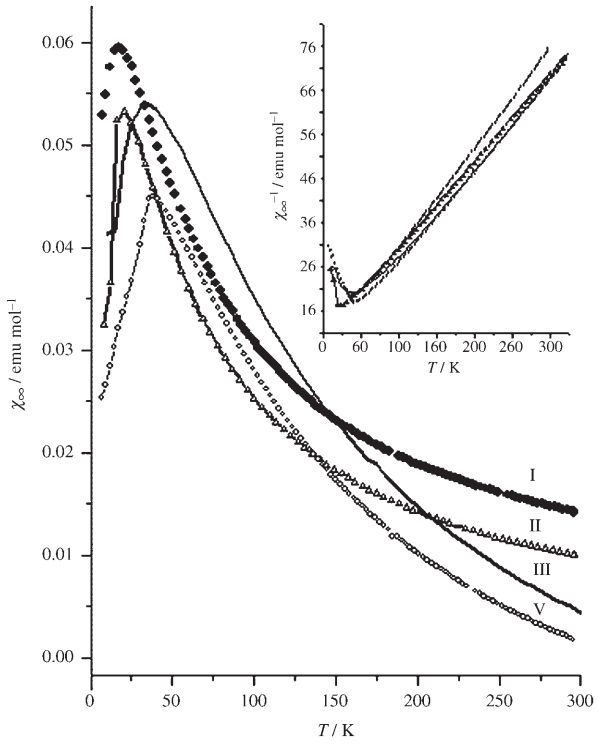

Figure 12. Temperature dependence of magnetic susceptibility for compounds **I**–**III** and **V**. The inset shows the temperature variation of the inverse susceptibility.

Table 3. The various magnetic parameters for the compounds **I**–**III** and **V**.

Compound	C [Cm^3Kmol^{-1}]	θ_p [K]	T_N [K]	μ_{eff} [BM]
I	4.97	−25	18	6.08
II	3.55	−32	22	5.05
III	4.47	−68	34	5.40
V	4.79	−93	42	5.46

the oxalate units connect the iron phosphite inorganic layers in an out-of-plane fashion and complete the three-dimensional connectivity. In **V**, the oxalate unit performs the unusual dual role of satisfying the coordination requirements of the octahedral iron and providing the required anionic charge for the framework structure. In **VI**, the oxalate units have both in-plane and out-of-plane connectivity and perform another type of dual role. The observation of antiferromagnetic interactions in all cases shows that superexchange is facilitated through both the oxalate and the phosphite groups.

Experimental Section

The iron phosphite–oxalates **I**–**VI** were synthesized under hydrothermal conditions from a mixture containing a source of iron (simple salt or metal powder), H_3PO_3, oxalic acid and/or HF, and an organic amine. The various synthesis conditions employed in the present study are presented in Table 4. In all cases, the reaction mixtures were homogenized for ≈30 min at room temperature and heated in a 23-mL PTFE-lined stainless steel acid digestion bomb (final fill factor of ≈40%) for various times at various temperatures. The resulting products, which predominantly contained good-quality single crystals suitable for single-crystal X-ray diffraction, were filtered and washed thoroughly with deionized water. Thus, colorless rodlike (**I**), brown platelike (**II**), colorless platelike (**III**), brown platelike (**IV**), colorless platelike (**V**), and brown cubelike (**VI**) crystals were obtained. The products of the compounds **IV** and **VI** contain unreacted Fe powder as an impurity along with the brown-colored single crystals. In spite of several repeated attempts, we were not able to prepare **IV** and **VI** in pure form and hence, other than the single-crystal structure, we were not able to characterize those two compounds satisfactorily.

Initial characterizations were carried out by elemental analysis, energy dispersive X-ray analysis (EDAX), powder X-ray diffraction (XRD), thermogravimetric analysis (TGA), and IR spectroscopy studies. Elemental analyses of the crystals were carried out by using atomic absorption spectroscopy (ThermoFinnigan FLASH EA 1112 CHNS analyzer). Elemental analysis: calcd (%) for **I**: C 25.61, H 4.02, N 7.50; found: C 25.08, H 4.52, N 7.02; calcd (%) for **II**: C 21.78, H 4.48, N 9.24; found: C 21.20, H 4.36, N 8.54; calcd (%) for **III**: C 25.61, H 4.02, N 7.50; found: C 25.08, H 4.52, N 7.02; calcd (%) for **V**: C 11.28, H 2.84, N 3.76; found: C 11.33, H 2.92, N 4.85. An EDAX analysis on many single crystals indicated Fe:P ratios of 1:1 for **I**, 2:1 for **II**, 1:1 for **III** and **IV**, 3:4 for **V**, and 2:1 for **VI**, results that are consistent with the single-crystal X-ray data.

The powder X-ray diffraction (XRD) patterns were recorded on crushed single crystals in the 2θ range 5–50° by using $Cu_{K\alpha}$ radiation (Philips X'pert Pro). The XRD patterns indicated that the products were new and were entirely consistent with the structures determined from the single-crystal XRD.

TGA studies have been carried out (Mettler-Toledo, TG850) in an oxygen atmosphere (flow rate = 50 mL min^{-1}) in the temperature range 25–800 °C (heating rate = 5 °C min^{-1}). The results indicated a two-step weight loss in the case of compounds **I**–**III** and **V**. The first weight loss (observed: 4.28% for **I**, 7.89% for **II**, 4.81% for **III**, and 6.15% for **V**), occurring at around 100–175 °C, corresponds to the loss of lattice water molecules (calcd: 4.64% for **I**, 7.42% for **II**, 4.35% for **III**, and 4.83% for **V**). The extra weight loss in the case of **V** may be due to some adsorbed water. The second weight loss (observed: 55.75% for **I**, 52.08% for

Table 4. Synthesis conditions for compounds **I**–**VI**.

Molar ratio	Synthesis conditions T [°C][a]	t [h]	Initial pH	Final pH	Yield [%]	Composition
FeC_2O_4:2 H_3PO_3:2 DABCO:2 HF:200 H_2O	150	72	2	2	80	$[C_6N_2H_{14}]_2[Fe^{III}_2(HPO_3)_2F_2(C_2O_4)_2]\cdot 2H_2O$ (**I**)
$FeCl_3$:2 H_3PO_3:$H_2C_2O_4$:2 TREN:122 H_2O	110	72	4	4	70	$[C_6N_4H_{21}]_2[Fe^{II}_4(HPO_3)_2(C_2O_4)_5]\cdot 5H_2O$ (**II**)
$FeCl_3\cdot 6H_2O$:2 H_3PO_3:$H_2C_2O_4$:En:122 H_2O	110	96	2	2	75	$[Fe_2^{III}(OH_2)_2(HPO_3)_2(C_2O_4)]\cdot H_2O$ (**III**)
Fe:2 H_3PO_3:$H_2C_2O_4$:En:122 H_2O	125	96	2	2	20	$[C_2N_2H_{10}][Fe^{II}_2(OH_2)_2(HPO_3)_2(C_2O_4)]$ (**IV**)
$FeCl_3\cdot 6H_2O$:2 H_3PO_3:$H_2C_2O_4$:BAPEN:122 H_2O	110+150	96+24	2	2	75	$[C_8N_4H_{26}][Fe^{III}_6(HPO_3)_8(C_2O_4)_3]\cdot 4H_2O$ (**V**)
Fe:2 H_3PO_3:$H_2C_2O_4$:Homopip:122 H_2O	125+150+180	96+48+24	2	2	15	$[C_5N_2H_{14}][Fe^{II}_4(HPO_3)_2(C_2O_4)_3]$ (**VI**)

[a] En = Ethylenediamine, BAPEN = *N*,*N*′-(3-bisaminopropyl)-1,2-ethylenediamine, Homopip = homopiperazine.

II, 24.52% for **III**, and 24.72% for **V**), occurring in the temperature range 250–600°C, corresponds to the loss of oxalate units and amine molecules and/or loss of coordinated water molecules (calcd: 53.93% for **I**, 60.94% for **II**, 29.25% for **III**, and 29.69% for **V**). The fluoride ion also leaves from **I**, along with the amine and oxalate units. It is likely that the water molecules formed during the combustion of the organic molecules hydrolyze the fluoride ion in the framework, thereby resulting in the formation of volatile hydrogen fluoride. It is clear that the calculated and observed weight losses differ considerably in all cases: for **I**, the total calculated weight loss (loss of lattice water, decomposition of oxalate units and amines, and condensation of the fluoride ion) is 64.05% (observed: 60.03%); for **II**, it is 68.41% (observed: 59.97%); for **III**, it is 34.30% (observed: 29.33%); for **V**, it is 34.52% (observed: 30.88%). The difference between the observed and calculated weight losses can be explained by considering the oxidation of P^{III} to P^{V} for all cases and Fe^{II} to Fe^{III} for **II**, during the decomposition process. The calculated weight gains for the oxidation of P^{III} to P^{V} are 4.13% for **I**, 5.27% for **II**, 7.72% for **III**, and 8.60% for **V**. The calculated weight gain for the oxidation of Fe^{II} to Fe^{III} is 3.95% for **II**. From a combination of these, the weight losses would be: for **I**, 64.16% (60.03+4.13; calcd: 64.05%); for **II**, 69.19% (59.97+5.27+3.95; calcd: 68.41%); for **III**, 37.05% (29.33+7.72; calcd: 34.30%); for **V**, 39.48% (30.88+8.60; calcd: 34.52%). These values are closer to the expected weight losses. In all cases, the final decomposed products were poorly crystalline and showed X-ray patterns corresponding to iron phosphate; $Fe^{III}PO_4$ (JCPDS: 01-084-0876) for **I**, $Fe^{III}_3PO_7$ (JCPDS: 00-037-0061) for **II**, $Fe^{III}_3(PO_4)_2$ (JCPDS: 00-027-0250) for **III**, and $Fe^{III}PO_4$ (JCPDS: 00-003-0379) for **V**.

IR spectroscopy studies were carried out in the range $\tilde{\nu}=400$–$4000\ cm^{-1}$ by using the KBr pellet method (Perkin–Elmer, SPECTRUM 1000 instrument). The IR spectra exhibited typical peaks corresponding to the amine molecule, the oxalate unit, the HPO_3 moiety, and the lattice water molecule with little variation in the respective bands. IR (KBr): $\nu_s=$ 3515–3525 cm^{-1} (H_2O), $\nu_s=3015$–$3350\ cm^{-1}$ (N–H), $\nu_s=2850$–$3075\ cm^{-1}$ $(C–H)_{asym}$, $\nu_s=2825$–$2970\ cm^{-1}$ $(C–H)_{sym}$, $\nu_s=2370$–$2408\ cm^{-1}$ (P–H), $\delta_{as}=1620$–$1642\ cm^{-1}$ (H_2O), $\nu_s=1655$–$1690\ cm^{-1}$ (C–O), $\nu_s=1515$–$1605\ cm^{-1}$ (N–H), $\delta_s=1460$–$1480\ cm^{-1}$ (C–H), $\delta_s=1405$–$1430\ cm^{-1}$ (C–O), $\nu_s=1100$–$1160\ cm^{-1}$ (C–N), $\nu_{as}=1023$–$1140\ cm^{-1}$ (P–O), $\delta_{as}=985$–$1050\ cm^{-1}$ (P–H), $\nu_s=865$–$1010\ cm^{-1}$ (P–O), $\delta_s=570$–$610\ cm^{-1}$ (P–O), $\delta_{as}=450$–$500\ cm^{-1}$ (P–O).

Measurement of the temperature variation of the magnetic susceptibility studies was carried out on powdered single crystals in the range 5–320 K with a SQUID magnetometer (Quantum Design, USA).

Single-crystal structure determination: A suitable crystal for each compound was carefully selected under a polarizing microscope and glued to a thin glass fiber. The single-crystal diffraction data were collected on a Bruker AXS Smart Apex CCD diffractometer at 293(2) K. The X-ray generator was operated at 50 kV and 35 mA with $Mo_{K\alpha}$ ($\lambda=0.71073$ Å) radiation. Data were collected with a ω scan width of 0.3°. In total, 606 frames were collected in 3 different settings of ϕ (0, 90, and 180°) with the sample-to-detector distance fixed at 6.03 cm and the detector position (2θ) fixed at −25°. Pertinent experimental details of the structure determination of **I**–**VI** are presented in Table 5.

The data were reduced by using the SAINTPLUS software,[27] and an empirical absorption correction was applied by using the SADABS program.[28] The crystal structure was solved and refined by using SHELXL97,[29] present in the WinGx suite of programs (Version 1.63.04a).[30] The hydrogen atom on the P–H group and the hydrogen positions of the amine molecules in compounds **I**, **IV**, and **V** were located in the difference Fourier map. The lattice water molecules of **I**–**III** and **V**, one of the carbon atoms of the amine molecule of **II**, and the amine molecule of **VI** were found to be disordered. The location of the hydrogen positions for these molecules was not feasible. For the final refinement, the hydrogen atoms were placed in geometrically ideal positions and refined by using the riding mode. Isotropic refinements were

Table 5. Crystal data and structure refinement parameters for compounds **I**–**VI**.[a]

	I	**II**	**III**	**IV**	**V**	**VI**
empirical formula	$C_{16}H_{34}N_4O_{16}F_2P_2Fe_2$	$C_{22}H_{54}N_8O_{31}P_2Fe_4$	$C_1H_3O_{6.5}P_1Fe_1$	$C_2H_8N_1O_6P_1Fe_1$	$C_{14}H_{42}N_4O_{40}P_8Fe_6$	$C_{11}H_{16}N_2O_{18}P_2Fe_4$
F_w	750.186	1212.232	206.866	228.907	1489.565	749.570
crystal system	monoclinic	triclinic	monoclinic	monoclinic	monoclinic	monoclinic
space group	$P2(1)/n$ (no. 14)	$P\bar{1}$ (no. 2)	$P2(1)/c$ (no. 14)	$P2(1)/c$ (no. 14)	$P2(1)/n$ (no. 14)	$P2(1)/c$ (no. 14)
crystal size [mm]	0.20×0.10×0.08	0.16×0.12×0.10	0.20×0.10×0.08	0.20×0.12×0.10	0.14×0.10×0.12	0.12×0.10×0.10
a [Å]	12.511(16)	8.719(2)	4.875(10)	7.684(4)	8.473(10)	7.682
b [Å]	6.372(8)	8.827(2)	17.707(2)	8.651(4)	16.685(2)	7.726
c [Å]	33.153(4)	15.908(4)	6.984(2)	10.053(5)	16.214(3)	18.092
α [°]	90	78.617(4)	90.00	90.00	90.000	90.000
β [°]	90.532	84.047(4)	106.728(2)	100.821(8)	95.919(10)	94.443(2)
γ [°]	90	68.241(4)	90.00	90.00	90.000	90.000
V [Å^3]	2643.0(6)	1114.1(6)	577.46(2)	653.6(5)	2280.35(6)	1070.8(3)
Z	4	2	4	4	4	4
T [K]	293	293	293	293	293	293
ρ_{calcd} [g cm^{-3}]	1.875	1.770	2.368	2.317	2.157	2.004
μ [mm^{-1}]	1.317	1.456	2.857	2.525	2.261	1.589
λ [Å]	0.71073	0.71073	0.71073	0.71073	0.71073	0.71073
θ range [°]	1.73–27.99	2.52–28.07	2.30–27.96	2.70–27.95	2.44–28.03	2.26–27.99
reflections collected	22422	12872	4879	3769	19423	8974
unique reflections	6249	5156	1356	1518	5365	2538
number of parameters	379	309	99	109	334	172
GOF	1.203	1.064	1.136	1.029	1.070	1.053
R index [$I>2\sigma(I)$]						
R_1	0.1049	0.0430	0.0290	0.0414	0.0351	0.0376
wR_2	0.1805	0.1295	0.0682	0.1047	0.0961	0.0993
R (all data)						
R_1	0.1553	0.0590	0.0333	0.0461	0.0425	0.0394
wR_2	0.1981	0.1337	0.0699	0.1073	0.1003	0.1006
largest diff. peak and hole [e Å^{-3}]	0.835 and −0.764	0.711 and −0.666	0.607 and −0.388	0.976 and −0.805	1.502 and −0.476	1.740 and −0.892

[a] $R_1=\Sigma||F_o|-|F_c||/\Sigma|F_o|$; $wR_2=\{\Sigma[w(F_o^2-F_c^2)]/\Sigma[w(F_o^2)^2]\}^{1/2}$; $w=1/[\rho^2(F_o)^2+(aP)^2+bP]$; $P=[\max.(F_o, O)+2(F_c)^2]/3$, in which $a=0.0447$ and $b=14.8149$ for **I**, $a=0.0691$ and $b=0.9543$ for **II**, $a=0.0276$ and $b=0.8074$ for **III**, $a=0.0675$ and $b=0.0000$ for **IV**, $a=0.0434$ and $b=7.2045$ for **V**, and $a=0.0537$ and $b=2.9382$ for **VI**.

employed for the disordered atoms. The last cycles of refinement included atomic positions and anisotropic thermal parameters for all of the non-hydrogen atoms. Full-matrix-least-squares structure refinement against $|F|^2$ was carried out by using the WinGx[30] package of programs. CCDC 611556–611560 (compounds **I**–**V**) and 297880 (compound **VI**) contain the supplementary crystallographic data for this paper. These data can be obtained free of charge from the Cambridge Crystallographic Data Centre via www.ccdc.cam.ac.uk/data_request/cif.

Acknowledgements

We thank DST-IRHPA (India) for the CCD facility. S.N. gratefully acknowledges the generous support of the Department of Science and Technology (DST) and the Council of Scientific and Industrial Research (CSIR), Government of India, through the award of research grants.

[1] A. K. Cheetham, T. Loiseau, G. Ferey, *Angew. Chem.* **1999**, *111*, 3466–3492; *Angew. Chem. Int. Ed.* **1999**, *38*, 3268–3292.
[2] L. E. Gorden, W. T. A. Harrison, *Inorg. Chem.* **2004**, *43*, 1808–1809.
[3] J. Liang, Y. Wang, J. H. Yu, Y. Li, R. R. Xu, *Chem. Commun.* **2003**, 882–883.
[4] S. Fernandez-Armas, J. L. Mesa, J. L. Pizarro, J. S. Garitaonandia, M. I. Arrortua, T. Rojo, *Angew. Chem.* **2004**, *116*, 995–998; *Angew. Chem. Int. Ed.* **2004**, *43*, 977–980.
[5] S. Mandal, M. A. Green, S. Natarajan, *Current Science* **2005**, *11*, 1899–1903.
[6] S. Fernandez, J. L. Mesa, J. L. Pizarro, L. Lezama, M. I. Arriortua, T. Rojo, *Chem. Mater.* **2002**, *14*, 2300–2307.
[7] S. Fenandez, J. L. Mesa, J. L. Pizarro, L. Lezama, M. I. Arriortua, T. Rojo, *Angew. Chem.* **2002**, *114*, 3835–3837; *Angew. Chem. Int. Ed.* **2002**, *41*, 3683–3685.
[8] A. Choudhury, S. Natarajan, C. N. R. Rao, *Chem. Eur. J.* **2000**, *6*, 1168–1175.
[9] A. Choudhury, S. Natarajan, *J. Mater. Chem.* **1999**, *9*, 3113–3117.
[10] A. Choudhury, S. Natarajan, C. N. R. Rao, *Chem. Mater.* **1999**, *11*, 2316–2318.
[11] Y.-C. Jiang, S.-L. Wang, K. H. Lii, N. Nguyan, A. Ducouret, *Chem. Mater.* **2003**, *15*, 1633–1638.
[12] S. Mandal, S. K. Pati, M. A. Green, S. Natarajan, *Chem. Mater.* **2005**, *17*, 2912–2917.
[13] C. N. R. Rao, S. Natarajan, R. Vaidhyanathan, *Angew. Chem.* **2004**, *116*, 1490–1521; *Angew. Chem. Int. Ed.* **2004**, *43*, 1466–1496.
[14] S. Natarajan, *J. Solid State Chem.* **1998**, *139*, 200–203.
[15] T. Berrocal, J. L. Mesa, J. L. Pizarro, M. K. Urtiaga, M. I. Arriortua, T. Rojo, *J. Solid State Chem.* **2006**, *179*, 1659–1667.
[16] S. Charakbarti, S. Natarajan, *Angew. Chem.* **2002**, *114*, 1272–1274; *Angew. Chem. Int. Ed.* **2002**, *41*, 1224–1226.
[17] Y.-M. Tsai, S.-L. Wang, C.-H. Huang, K.-H. Lii, *Inorg. Chem.* **1999**, *38*, 4183–4187.
[18] S. Mandal, S. K. Pati, M. A. Green, S. Natarajan, *Chem. Mater.* **2005**, *17*, 638–643.
[19] R. Vaidhyanathan, S. Natarajan, A. K. Cheetham, C. N. R. Rao, *Chem. Mater.* **1999**, *11*, 3636–3642.
[20] Y.-C. Jiang, S.-L. Wang, S.-F. Lee, K.-H. Lii, *Inorg. Chem.* **2003**, *42*, 6154–6156.
[21] J. Fan, B. E. Hanson, *Inorg. Chem.* **2005**, *44*, 6998–7008.
[22] S. Neeraj, S. Natarajan, *J. Mater. Chem.* **2000**, *10*, 1171–1175.
[23] S. Mandal, S. Natarajan, *Solid State Sci.* **2006**, *8*, 388–396.
[24] G. Ferey, *Chem. Mater.* **2001**, *13*, 3084–3098.
[25] A. Choudhury, S. Natarajan, C. N. R. Rao, *J. Solid State Chem.* **1999**, *146*, 538–545.
[26] A. Choudhury, S. Natarajan, *Solid State Sci.* **2000**, *2*, 365–372.
[27] SMART (Ver. 5.628), SAINT (Ver. 6.45a), XPREP, SHELXTL, Bruker AXS Inc., Madison, WI, USA, **2004**.
[28] Siemens Area Correction Absorption Correction Program, G. M. Sheldrick, University of Göttingen, Göttingen, Germany, **1994**.
[29] SHELXL-97, Program for Crystal Structure Solution and Refinement, G. M. Sheldrick, University of Göttingen, Göttingen, Germany, **1997**.
[30] J. L. Farrugia, *J. Appl. Crystallogr.* **1999**, *32*, 837–838.

Received: July 18, 2006
Published online: October 25, 2006

